RSC Pharmaceutics

ROYAL SOCIETY OF CHEMISTRY

PAPER

View Article Online
View Journal



Cite this: DOI: 10.1039/d5pm00233h

# Controlled delivery of IL-10 and retinoic acid for the treatment of psoriasis using a multilayered microneedle

Nathaniel Wright, [a] Priya Bhashyam,[a] Lea Seo,[a] Tim Wu,[a] Alexander I. McGurk,[b] Marinel Ocasio-Rivera,[b] Anthony R. D'Amato,[a] Deborah J. Fowell[b] and Yadong Wang *[a]

Psoriasis is a chronic autoimmune disease driven by a proinflammatory feedback cycle that deteriorates normal skin function and structure. Current treatments often provide incomplete skin clearance or require systemic immunosuppression, which elevates the risk of infection and development of cancers. Here we report a novel dual modality immunotherapy delivered to a spatially localized target that avoids systemic exposure. We combined the cytokine interleukin-10 and the small molecule all-*trans* retinoic acid for the treatment of psoriasis, delivered in a single microneedle patch. The treatment improved psoriasis area and severity index scores and local biomarkers measured through histology, immunofluorescence, and flow cytometry. Ultimately, this study provides a foundation for the localized delivery of immunotherapeutics for psoriasis.

Received 29th August 2025,
Accepted 15th April 2026

DOI: 10.1039/d5pm00233h

rsc.li/RSCPharma



## 1. Introduction

Psoriasis is a cutaneous autoimmune disease that affects approximately 2% of the world population.[1–3] Plaque psoriasis, the most prevalent form of the disease, is characterized by the dysregulation of IL-23/IL-17 axis, driven by the complex interplay of T cells, antigen presenting cells, neutrophils, and keratinocytes. Specifically, Th17 cells drive the hyperproliferation of keratinocytes through the release of pro-inflammatory cytokines, notably IL-17A.[4] In turn, keratinocytes release antimicrobial peptides that in combination with inflammatory cytokines promote the chemotaxis of neutrophils and monocytes to the local tissue.[2,4–6] These recruited cells further stimulate T cell activity, perpetuating disease progression in an inflammatory cycle.

Given the therapeutic potential of interleukin 10 (IL-10) and all-*trans* retinoic acid (ATRA), we developed a locally delivered immunotherapy to treat the affected skin in the imiquimod (IMQ) mouse model. IL-10 is a pleiotropic cytokine that acts as a master regulator of immune homeostasis, suppressing monocytes, macrophages, and $CD4^+$ T cells while promoting peripheral tolerance.[7–9] Although previous clinical studies have shown IL-10 to be well tolerated, its efficacy was variable, with high systemic dosages (20 μg $kg^{-1}$) required for therapeutic effect.[10–12] While each of these topicals target various aspects of the disease, retinoids such as ATRA exert anti-inflammatory effects on immune cells and inhibits keratinocyte hyperproliferation.[13–16] ATRA can be delivered topically or orally but has limited efficacy seen as incomplete skin clearance after months of treatment.[3] Other therapeutics also fail to meet or maintain satisfactory skin clearance over time.[17–19] These underline the importance of finding an appropriate controlled release mechanism for IL-10 and ATRA.

We designed a novel immunomodulatory therapy that delivers therapeutics into a localized area thereby avoiding large scale systemic exposure. We used a coacervate microneedle patch for controlled release of IL-10 and ATRA. Given that previous studies utilized bolus injections of IL-10, we hypothesized that the simultaneous controlled delivery of IL-10 and ATRA would enhance the therapeutic effect of both compounds. Coacervation, a liquid–liquid phase separation, has been used for the controlled delivery of various cytokines and growth factors.[20–23] We used a poly(ethylene argininylaspartate diglyceride) (PEAD)/heparin coacervate system encapsulated within the first layer of the microneedle to protect IL-10 and control its release, thereby avoiding the rapid degradation of the cytokine *in vivo* and enabling sustained long-term dosing. The second layer of the microneedle was loaded with ATRA. Upon application, the rapid dissolution of the first layer releases the coacervate into the local tissue for controlled delivery of IL-10 from the coacervate with the slow release of ATRA from the microneedle.[24] The resultant microneedle therapy improved outcomes in the IMQ mouse model, as revealed by PASI score, histology, immunofluorescence, and cell infiltration. The decreases in key markers of disease progression

[a]*Nancy E. and Peter C. Meinig School of Biomedical Engineering, Cornell University, Kimball Hall 290, Ithaca, 14853 USA. E-mail: yw839@cornell.edu; Tel: +1-607-255-4030*
[b]*Department of Microbiology and Immunology, Cornell University, Ithaca, NY, USA*

demonstrate promise for local treatment of psoriasis with microneedles as anti-inflammatory immunotherapy.

## 2. Methods

### 2.1 Materials

The following materials were purchased and used: PEAD as previously synthesized,[25] sodium heparin (Scientific Protein Labs, WI, USA), sterile saline 0.9% (NaCl) (GROWCELLS, Irvine, CA, USA), Sylgard 184 Kit (Dow, Midland, MI, USA), bovine serum albumin (VWR, Radnor, PA, USA), ethanol (Decon Labs, PA, USA), recombinant mouse interleukin 10 (IL-10) (R&D Systems, MN, USA), all-*trans* retinoic acid (ATRA) (Enzo Life Sciences, Farmingdale, NY, USA), polyvinylpyrrolidone (PVP) 360 kDa (Sigma-Aldrich, MO, USA), ethyl cellulose (Grainger, NY, USA), poly(D,L-lactide-*co*-glycolide) 50 : 50 (Polysciences, PA, USA), murine IL-10 standard TMB ELISA development kit (VWR, Radnor, PA, USA), VERIGUIDE OS Resin (Whip Mix, Louisville, KY, USA), isopropyl alcohol (VWR, Radnor, PA, USA), imiquimod cream (Perrigo, MI, USA), Epredia™ Cryomatrix™ embedding resin (Fisher Scientific, Waltham, MA), CD31 monoclonal antibody (14-0311-82), TNF-α monoclonal antibody (14-7321-85), and anti-rat TRITC secondary antibody (Thermo Fisher, Waltham, MA).

### 2.2 Microneedle preparation

Microneedles were prepared as previously described.[24] Briefly, polyvinylpyrrolidone (PVP) was dissolved in sterile saline at 5% w/v. Poly(ethylene argininylaspartate diglyceride) (PEAD) and heparin were then separately added at 10 mg $mL^{-1}$ to PVP solution. IL-10 was added to the heparin/PVP solution to allow for binding to the glycosaminoglycan prior to the addition of PEAD/PVP solution at a final mass ratio of 3.6 : 1 PEAD : heparin. Immediately following coacervate formation, the first layer of the microneedles was made through vacuuming and then drying the needles. The subsequent layer was made from a 15/85 (w/w) blend of poly(lactic-*co*-glycolic acid) (PLGA) and ethyl cellulose (EC) selected for compatibility with the fabrication process. ATRA was kept out of light and added to the PLGA/EC solution. The solution was used to generate microneedle patches with 10 μg of ATRA.

### 2.3 SEM images of microneedles

Microneedles were first sputter coated with 10 nm of Au–Pd prior to imaging with the SEM. Images were taken using a NeoScope™ Benchtop SEM, JCM-7000. Scale bars were added using ImageJ.

### 2.4 Axial and transversal testing of microneedles

Microneedles were made using varying amounts of PVP in saline from 2.5 to 10% w/v with or without coacervate. Groups containing coacervate were made using a PEAD : heparin of 3.6 : 1. Analysis of the failure for each sample was measured using an Instron 5943 with a 50 N load cell. Instron platforms were positioned parallel to each other with the microneedle patch flat across the center. The top platform was brought into contact with the needles of the microneedle patch prior to beginning compression experiments. Failure points were collected for each group ($N = 8$) at the point of needle failures.

### 2.5 IL-10 controlled release from microneedles

Microneedles were prepared with 200 ng of recombinant murine IL-10 in a single patch without any ATRA to avoid spectral interference from the small molecule. Complex coacervates were prepared with 200 ng recombinant murine IL-10 following previously described protocols. Then, patches were incubated at 37° for 30 days. On days 0, 1, 2, 3, 4, 5, 6, 7, 8, 10, 12, 14, 16, 19, 23, 27, and 30 samples were removed from the incubator, spun down at 12 100 RCF, and the supernatant replaced then frozen prior to analysis by ELISA.

IL-10 was recovered from prepared microneedles using a PBS solution to rapidly dissolve the PVP and collect the encapsulated protein. After collection, proteins were isolated from PVP using Sartorius Vivaspin columns. Stock protein was compared using a JASCO 1500 CD spectrometer to collected samples. Measurements were taken from 250–200 nm, at a rate of 50 nm $min^{-1}$ for three iterations at 0.1 mg $mL^{-1}$.

### 2.6 IMQ mouse model experimental design

All animal procedures were performed in accordance with the Guide for Care and Use of Laboratory Animals of Cornell University, including the IMQ Mouse Model and subsequent experiments and animal sacrifice for histological and flow cytometry analyses. All procedures were approved by the Cornell Institutional Animal Care and Use Committee (IACUC Protocol 2018-0033) prior to being conducted.

Imiquimod (IMQ) is a TLR7/8 agonist commonly used to induce a psoriasiform phenotype in mice.[26,27] Mice were shaven days prior to the beginning of the experiment. To induce and maintain the psoriaform skin, 62.5 mg of 5% IMQ cream was applied over an area of 5 $cm^2$ starting on day 1, and for a total of 8 days on the flank of C57BL/6 mice 6–8 weeks of age. PASI scores were recorded daily for 8 days following application. Six experimental groups were followed during the 8-day application period as shown below. Treatment began on day 2 (Table 1).

On days 4 and 8, blood samples were taken from the subcutaneous vein, additionally, one mouse per group was euthanized by $CO_2$ to collect skin samples. Tissues were either dissociated and homogenized for further analysis *via* ELISA or used for histological sectioning. Tissues for sectioning were fixed in 4% PFA and then stored overnight at 4 °C in 30% sucrose solution. Tissue was then frozen in Epredia™ Cryomatrix™ embedding resin prior to sectioning on the Cryostar NX70. Sections were cut at 8 μm thickness and placed onto glass slides.

### 2.7 Histology and immunostaining

Excess OCT was removed with a PBS wash prior to staining. Samples were stained with hematoxylin and eosin (H&E), Masson's trichrome, and antibodies for immunofluorescence. H&E staining was done following standardized protocols for OCT embedded samples. Masson's trichrome was done through Animal Health Diagnostic Center at Cornell

**Table 1** *In vivo* groups for PASI scoring and tissue collection. All but the naïve group received imiquimod cream to induce psoriasiform skin. Treatment type, dosage, and route are also described

| Group name | IMQ applied | IL-10 dosage/form | RA dosage/form | Delivery route |
|---|---|---|---|---|
| Naïve | No | None | None | Untreated |
| Imiquimod | Yes | None | None | Control |
| RA cream | Yes | None | 10 μg RA | Topical |
| IL-10 bolus + RA cream | Yes | 4 μg IL-10 (soluble) | 10 μg RA (cream) | Subcutaneous + topical |
| IL-10 Coacervate bolus + RA cream | Yes | 4 μg IL-10 (coacervate) | 10 μg RA (cream) | Subcutaneous injection + topical |
| Microneedle treated | Yes | 4 μg IL-10 (coacervate microneedle) | 10 μg RA (microneedle) | Multilayered microneedle |

University. Immunofluorescence was carried out as follows; CD31 (Invitrogen), and TNF-α (Invitrogen) were diluted at a rate of 1 : 100, 1 : 100, and 1 : 20 respectively. CD31 and TNF-α were then counterstained with an anti-rat IgG, Tritc (Invitrogen) and CD3 stained with anti-Armenian Hamster, Alexa Fluor 488. DAPI was applied to the slides for 5 minutes and washed off prior to coverslip placement. Images were taken using a Nikon T2 Eclipse inverted microscope. Both fluorescent and bright field images were taken using 20× objectives (40× magnification).

### 2.8 Image analysis

Images were analyzed using ImageJ. H&E and Masson's trichrome stains were normalized using Reinhard normalization. Epidermal thickness was measured using H&E sections with three replicates across each group. Fluorescence was calculated following background subtraction from unstained areas. Mean fluorescence intensity was then calculated from within designated ROIs using the measurement function of ImageJ. Data was normalized to the control for each group to minimize any staining variation.

### 2.9 Flow cytometry of cells from treatment site

Three groups of C57BL/6 mice, from Jackson Labs, were analyzed with 5 mice per time point and tissue harvested on days 4 and 8. Mice were treated with imiquimod cream and euthanized following Cornell's IACUC protocols before harvesting skin. Skin samples were harvested, digested, filtered, and stained either with anti-CD45 BUV395 (1 : 500, 30-F11, BD Bioscience), anti-CD64 BV605 (1 : 200, X54-5/7.1, Biolegend), anti-CD11c BV711 (1 : 450, N418, Biolegend), antiCD19 BV786 (1 : 100, 1D3, BD Biosciences), anti-F4/80 PE-Cy5 (1 : 200, BM8, Invitrogen), anti-CD88 anti-APC (1 : 800, 20/70, Biolegend), anti-MHC-II APC-ef780 (1 : 2000, M5/114.15.2, eBioscience), anti-CD26 PE-Cy7 (1 : 150, H194-112, Biolegend), anti-XCR1 BV650 (1 : 200, ZET, Biolegend), anti-Ly6G FITC (1 : 500, 1A8, Biolegend), anti-CD4 BUV805 (1 : 500, 145-2C11, eBioscience), Ghost dye violet 510 dead cell stain (1 : 1000, Biolegend). Near-IR fluorescent reactive dye APC-Cy-7 dead cell stain (1 : 1000, Invitrogen), anti-CD45 BUV395 (1 : 200, 30-F11, BD Biosciences), anti-CD4 BUV805 (1 : 200, 145-2C11, eBioscience), anti-CD8b BV421 (1 : 200, X54-5/7.1, Biolegend), anti-Tbet BV711 (1 : 100, O4-48, BD Biosciences), anti-RORgT PE-CF594 (1 : 100, Q31-378, BD Biosciences), anti-IL-17a PE-Cy5.5 (1 : 100, TC11-18H10.1, Biolegend), anti-IFN-γ APC (1 : 100, XMG1.2, Biolegend), anti-FoxP3 Alexa Flour 488 (1 : 100, MF23, BD Biosciences) or with anti-CD45 BUV396 (1 : 250, IM7, BD Bioscience), anti-CD4 BUV805 (1 : 250, GK1.5, BD Bioscience), anti-CD64 BV605 (1 : 100, x54-5/7.1, BioLegend), Ghost Live/Dead BV510 (Tonbo Biosciences), anti-XCR1 BV650 (ZET, BD Bioscience), anti-CD11c BV711 (1 : 225, N418, BioLegend), anti-CD19 BV786 (1 : 250, 1d3, BD Bioscience), anti-Ly6G FITC (1 : 250, 1A8, BioLegend), anti-F4/80 PE-cy5 (1 : 100, BM8, Invitrogen), anti-CD26 PE-cy7 (1 : 75, H194-112, BioLegend), anti-CD88 APC (1 : 400, 20/70, BioLegend), and anti-MHCII APCef780 (1 : 750, M5/114, Invitrogen) prior to analysis on a FACSymphony A3 Analyzer.

### 2.10 Statistical analysis

Statistical analysis of data was completed using R (4.3.2) and PRISM 10. PASI score of all groups were compared using a one-way ANOVA followed by a *post hoc* Tukey test as the multiple comparison procedure. Error bars shown represent standard deviation and significance is determined from the Tukey test. Epidermal thickness measurement analysis was conducted in PRISM 10 using a one-way ANOVA followed by a *post hoc* Tukey test. Flow analysis was conducted in PRISM 10 using Student's *t* test. Error bars are shown with SEM. Analysis of MFI data was done using a two-ways Student's *t* test. Error bars are shown with SEM including propagated error from normalization.

## 3. Results

### 3.1 Coacervate microneedles maintain mechanical properties required to pierce the skin

Microneedles were fabricated with coacervate at a 10 mg $mL^{-1}$ concentration. Layered microneedles were fabricated using a previously described process: the first layer consisted of polyvinyl pyrrolidone (PVP) containing varying amounts of complex coacervate; and the second layer of a 15/85 (w/w) blend of poly (lactic-*co*-glycolic acid) (PLGA) and ethyl cellulose (EC). Polymers were selected based on biocompatibility, compatibility of the polymers with coacervate, and previous work within

the Wang lab (data not shown). The SEM images taken of the microneedles show a similar morphology to previous layered microneedles[24] (Fig. 1). The microneedles retained their obelisk shape with the pyramidal head improving skin penetration over conical heads.[28,29] Importantly, even with the incorporation of coacervate in the multilayered microneedle, they retained their previously observed morphology. Next, we verified the mechanical stability of the microneedles for skin penetration.

To further validate the addition of coacervate to microneedles we also examined the mechanical properties showing enough force to puncture skin (Fig. 2). Multiple concentrations of PVP were tested to ensure that microneedles met the minimum criteria for skin penetration. Microneedles were fabricated with 2.5, 5, or 10% PVP (w/v). After fabrication microneedles were subjected to Instron mechanical compression and the minimum force at failure was recorded. Eight microneedles were used for each group shown. In Fig. 2 the force required to break the needles for 2.5% PVP ($p < 0.05$) and 5% PVP ($p < 0.005$) was significantly decreased while there was a trending decrease in 10% PVP ($p > 0.05$). From this we conclude that the incorporation of the coacervate into the PVP matrix significantly impacts the ability of the needles to withstand mechanical force.

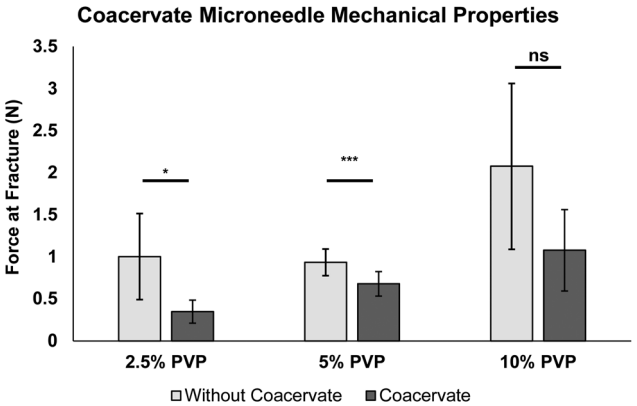


**Fig. 2** Microneedle fracture force indicates sufficient strength to pierce the skin. Measurements were taken using a compression test on microneedles ($n$ = 8) with an Instron. The amount of PVP used to fabricate microneedles ranged from 2.5% to 10% (w/v). Coacervate was introduced into the microneedles at 1% (w/v) and decreased the force required to fracture 2.5% and 5% PVP microneedles but was not significant for 10% PVP. SEM shown.

### 3.2 Controlled release of IL-10 from coacervate

The controlled release of interleukin-10 (IL-10) from coacervates displayed protein release over a 30-day period at 37 °C in

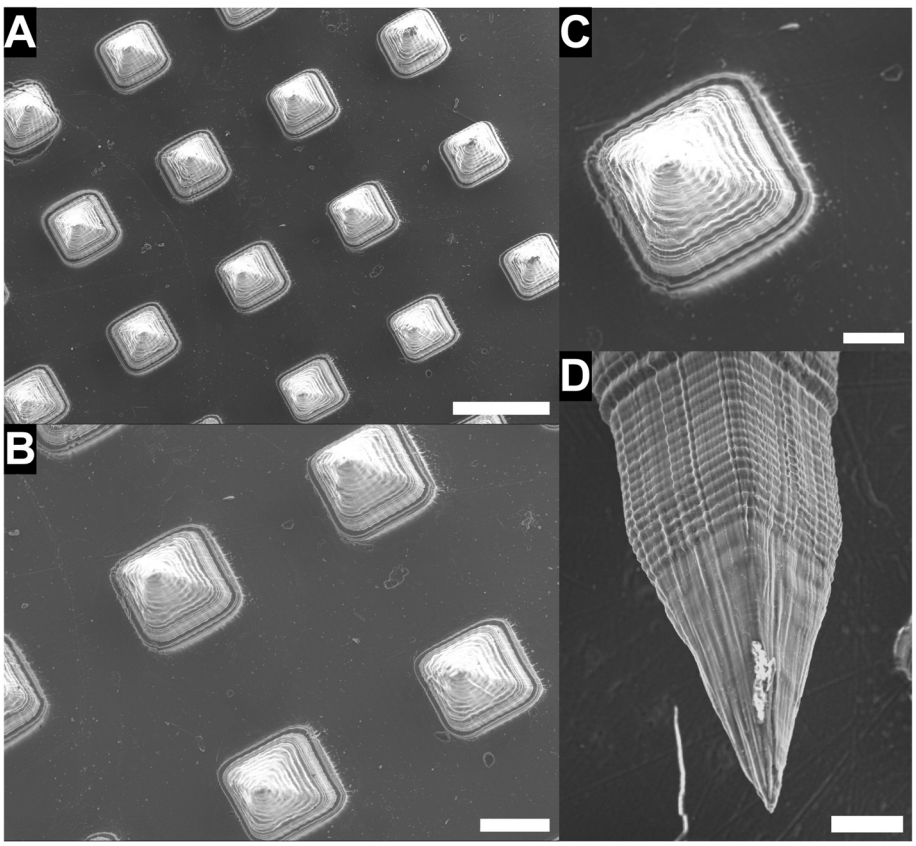


**Fig. 1** SEM images of microneedles loaded with recombinant murine IL-10 in coacervate and ATRA. (A) Wide view of microneedle patch, scale bar: 500 μm. (B) Focus on four needles of image A, scale bar: 200 μm. (C) Zoomed in image of B, scale bar: 100 μm. (D) Side profile of an individual microneedle, scale bar: 100 μm. The microneedle tips are sharp and pyramidal shaped heads matching the 3D master mold. The 3D printed master mold is used to fabricate the negative mold, giving rise to the layer lines seen on the microneedles.

saline, stabilized by 1% BSA (Fig. 3). There was a steady release of 71% of the total protein over the first 10 days followed by a slower release of another 18% over the subsequent 20 days. This sustained release of IL-10 demonstrates the potential for delivery across prolonged time frames.

### 3.3 Therapeutics loaded microneedles maintain efficacy *in vitro*

We evaluated the bioactivity of the active pharmaceutical ingredients after fabrication of the microneedles. IL-10 was encapsulated within our microneedles as previously described. Following fabrication, the protein was isolated before being analyzed with circular dichroism (CD) to examine the secondary structure of IL-10. After multiple runs ($N$ = 3), the previously encapsulated IL-10 and native IL-10 were analyzed using BestSel to investigate secondary structures.[30] This was used to determine no significant difference between groups (Fig. 4). We have previously reported the preservation of bioactivity of all-*trans* retinoic acid (ATRA) within a layered microneedle fabricated in the same manner,[24] thus we did not repeat the experiment here.

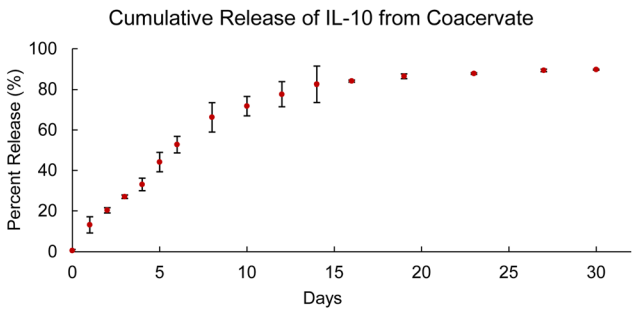


**Fig. 3** Controlled release of IL-10 encapsulated in PEAD/heparin coacervate ($n$ = 3). 89% of IL-10 that was loaded into the coacervate was released over the 30-day observation period. The initial 14 days showed a linear like release of IL-10 with 71% being released. This demonstrates the ability of coacervate to control the release of IL-10. SEM shown.

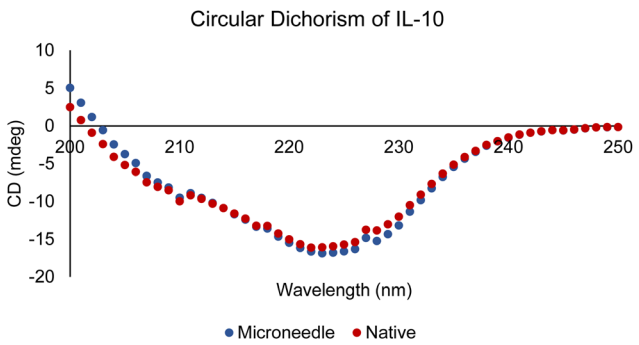


**Fig. 4** Circular dichroism spectra of IL-10 as a free protein and recovered after it was encapsulated in a microneedle. IL-10 recovered from the microneedle exhibits the same circular dichroism spectrum as the native IL-10, indicating an excellent preservation of the secondary structure of IL-10 throughout the microneedle fabrication process. Measurements conducted at 0.1 mg mL$^{-1}$.

### 3.4 Treatment improves psoriasis area and severity index score

The Psoriasis Area and Severity Index (PASI) is a tool for the measurement of three main markers of psoriasis; erythema, thickness, and scaling of the skin.[31] These measurements are given in a range of 0 or none to 4 or severe then subsequently summed into a final cumulative score. The scores provide healthcare professionals with a quantitative measurement of the disease progression and severity.[32] The imiquimod (IMQ) mouse model is a reproducible and reliable model of psoriasis that was used to investigate the therapeutic potential of the layer microneedles.[26]

PASI scores were recorded starting the day of IMQ application (day 1) until the last day (day 8). Treatment began on day 2 allowing for psoriasis to begin spreading unimpeded by treatment. The disease progression was seen in all groups treated with IMQ, however, groups that received treatment had lower PASI scores (Fig. 5). The coacervate and microneedle treatments had the most significant improvement on the disease whereas other treatments had less durable responses (Fig. 5). Bolus injection of IL-10 in combination with ATRA cream failed to achieve results comparable to the coacervate treatment highlighting the necessity of a controlled delivery method, consistent with many other cytokines. Given that all treatments were done with equivalent dosages, the impact of controlled delivery should be explored further.

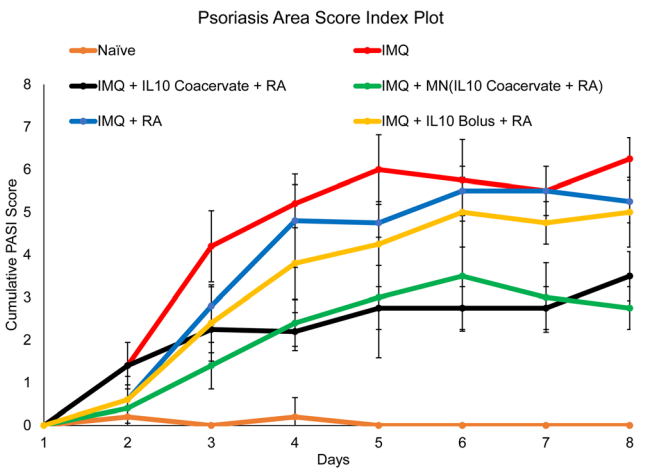


**Fig. 5** Cumulative PASI score index of IMQ treated mice ($n$ = 4). All treatments improved the disease symptoms. Two treatments stood out: microneedles loaded with IL-10 coacervate and RA, and RA cream combined with injection of IL-10 coacervate. On day 4, comparisons between groups and IMQ naïve control showed the following differences: RA cream ($p > 0.05$), bolus IL-10 and RA cream ($p < 0.05$), IL-10 coacervate and RA cream ($p < 0.001$), and microneedle treated ($p < 0.001$). On day 8 comparisons between groups and IMQ naïve control showed the following: RA cream ($p < 0.05$), bolus IL-10 and RA cream ($p > 0.05$), IL-10 coacervate and RA cream ($p < 0.01$), and microneedle treated ($p < 0.001$). These results highlight the importance of controlled release of IL-10 provided by coacervate and to some extent RA.

### 3.5 Histological impact of treatment on IMQ skin

On days 4 and 8 of the study, skin samples were collected, fixed, cryopreserved, and sectioned for histological analysis. H&E and Masson's trichrome staining were used to evaluate impact of treatment on disease pathology and immune cell infiltration into the local tissue. By day 4, rete ridges, long protrusions from the epidermis into dermal skin layers, were observed prominently in the IMQ groups with the formation of the ridges in other treatment groups (Fig. 6). By day 8, rete ridge formation had increased throughout all the groups; however, this change was notably less pronounced within the bolus coacervate, and microneedle treated groups. Despite some morphological changes, immune cell infiltration is seen throughout all IMQ treated groups. These results suggest that while treatment with IL-10 and ATRA may influence structural remodeling, it did not significantly reduce immune cell infiltration into the local environment.

Masson's trichrome staining was utilized to visualize keratinocyte hyperproliferation in the skin through the high contrast created between the red stained epidermis and the blue stained dermis (Fig. 7). As seen in the naïve group, the stratum corneum is a thin layer of non-nucleated material along the outermost edge of the skin. However, this is commonly dis-

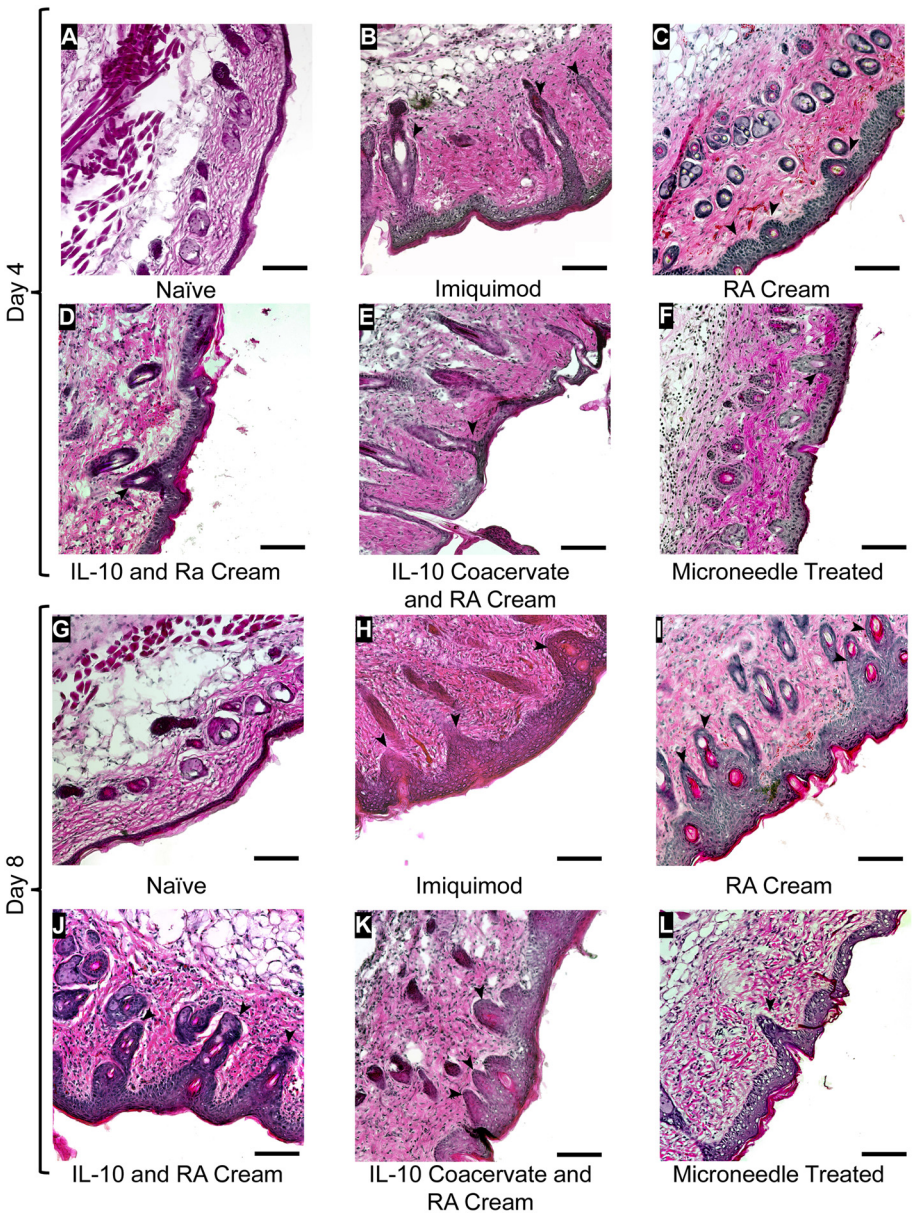


**Fig. 6** H&E images of treatment groups on days 4 and 8. Scale bars: 100 μm. On day 4 groups receiving treatment in addition to IMQ show decreases in epidermal thickening and rete ridge formation (A–F). By day 8, only the microneedle group showed a decreased epidermal thickening and a resistance to rete ridge formation (G–L). Rete ridge formation is denoted by black arrows. Scale bar: 100 μm.

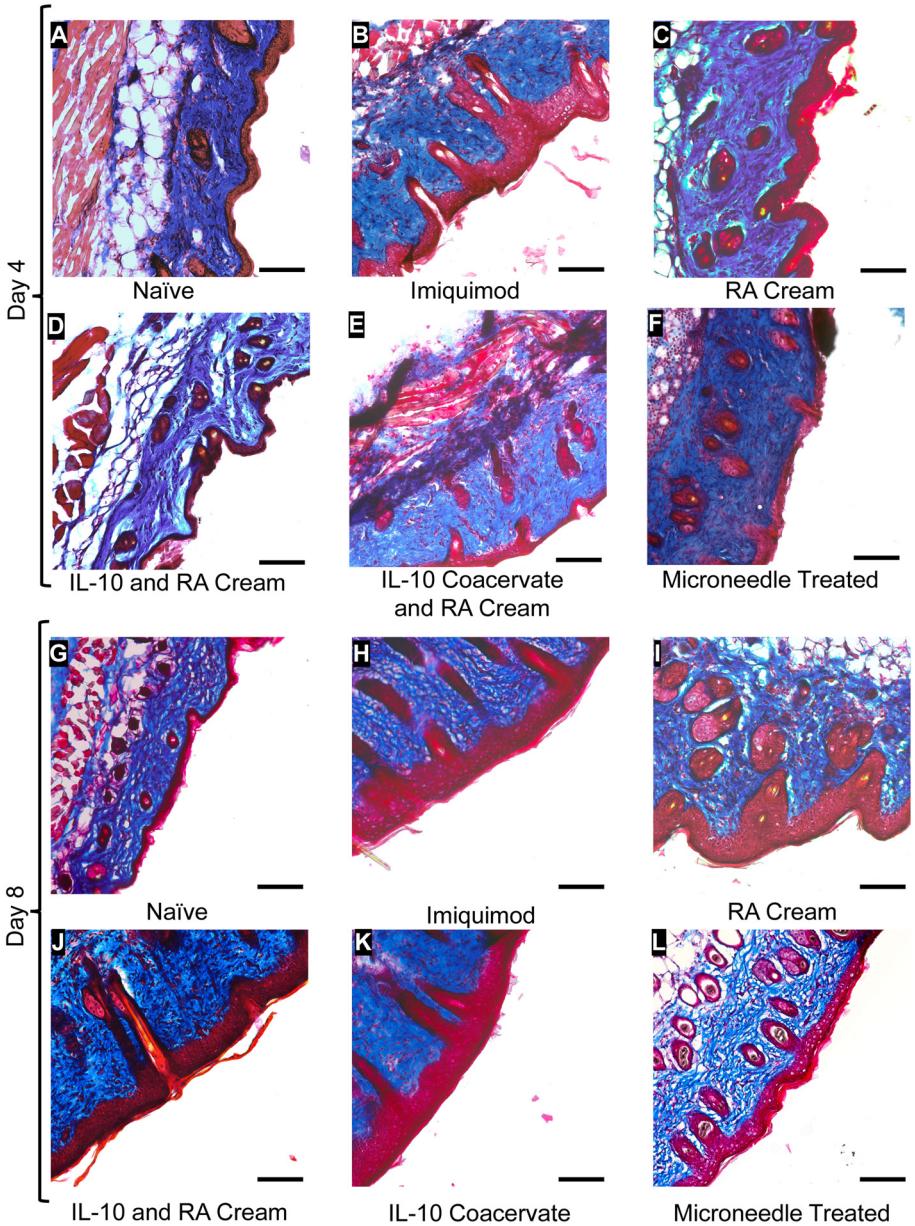


**Fig. 7** Tissues were harvested on day 4 (A–F) and day 8 (G–L), then embedded in OCT. Tissues were then sectioned and stained with Masson's trichrome. Resulting images show an increase in epidermal thickening across days. Scale bar: 100 μm.

rupted in the IMQ mouse model leaving only the hyperproliferated keratinocytes in the epidermis. As of day 4, all treatment groups had decreased skin thickening but was most pronounced in the bolus coacervate injection with RA cream (Fig. 7). Significant differences were identified between all treatment groups and the imiquimod skin control. A robust response to treatment was seen in all groups treated with IL-10, especially those containing coacervate, bolus, and microneedle treatments.

Using the H&E stained tissue samples, we quantified the epidermal thickening using ImageJ to measure thickening across multiple sections and completed analysis in GraphPad Prism (Fig. 8). The results followed the trends seen in PASI score tracking with increasing thickness across the experiment duration. While strong therapeutic responses were evident at day 4, the differences between most treatment groups and the imiquimod control became non-significant by day 8, except for both the coacervate and microneedle treatment groups which maintained a significant therapeutic effect (Fig. 8).

### 3.6 Impact of treatment on CD31 and TNF-α expression

To verify the expression levels of CD31 and TNF-α in mouse skin, immunofluorescence (IF) was performed on harvested

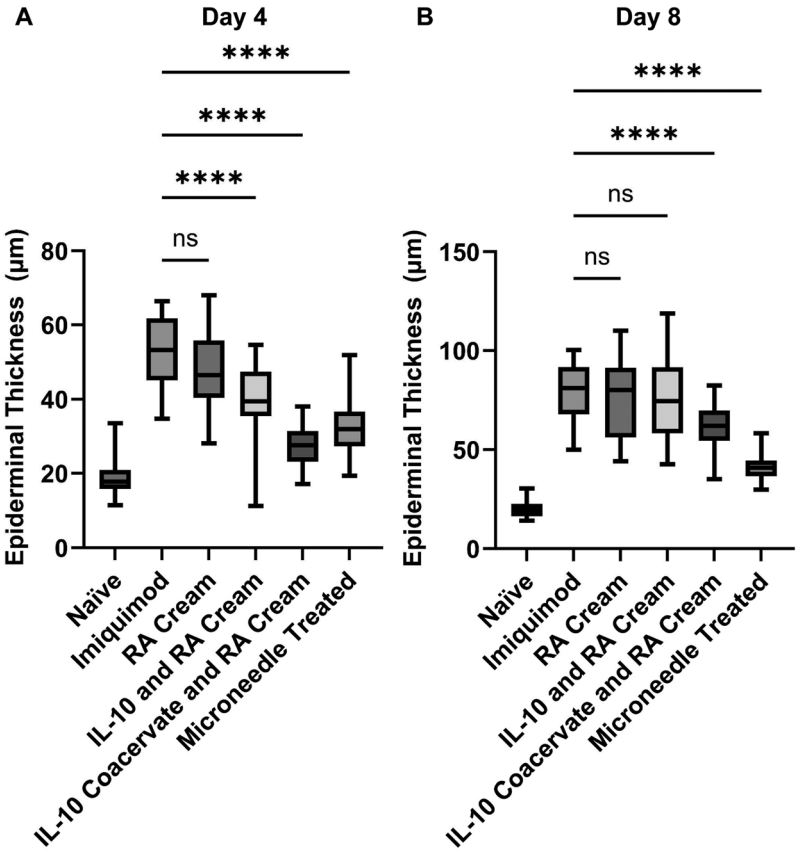


**Fig. 8** Analysis of epidermal thickening from H&E staining on day 4 (A) and day 8 (B). Analysis was conducted using a one-way ANOVA followed by *post hoc* Tukey test ($n$ = 30). Box plots of the resulting analysis are displayed with significance compared to the imiquimod treated group. Measurement ranges are shown.

tissues on day 4 (Fig. 9) and day 8 (SI Fig. S1). Following primary antibody application and secondary antibody application, nuclei were stained with DAPI, and sections were imaged on a TI2 Nikon inverted microscope. Image analysis revealed that treatments significantly reduced CD31 in IL-10 bolus and IL-10 Coacervate treatment groups at day 4 (SI Fig. S2). The microneedle treated group approached significance on day 4. By day 8 all three IL-10 treatment groups showed significantly reduced CD31 expression. Interestingly, on day 4 only the IL-10 coacervate group showed significant reduction in TNF-α. Only the IL-10 bolus treatment group showed significant reduction on day 8 with other two IL-10 groups trending towards significance. As CD31 facilitates both angiogenesis and leukocyte transmigration, these reductions are consistent with attenuation of local inflammatory and angiogenic markers. Additionally, a trending decrease in TNF-α lends itself to this conclusion. However, conclusions are limited by the temporal resolution.

### 3.7 Flow cytometry analysis of microneedle treatment on cell infiltration and populations within IMQ skin

To evaluate the impact of IL-10 and ATRA microneedles had on individual cell populations, we performed flow cytometry. Myeloid and T cell populations were specifically explored within these experiments based on previous work.[33] Mice received daily topical IMQ applications, with a cohort of mice treated with microneedles on day 2. Skin tissues were harvested on days 4 and 8 for analysis. Our results indicate a reduced inflammatory response to IMQ when treated with the IL-10 and ATRA microneedles, despite the initial influx of immune cells caused by microneedles (Fig. 10). There was a significantly lower frequency of $CD4^+$ T cells found within the tissue on day 8 following patch treatment with a highly variable number of Tregs. Both the number of neutrophils, monocytes and cDCs in the microneedle patch treated skin were higher on day 4. However, by day 8 we observed a higher monocyte and cDC cell number within the IMQ mice approaching significance with the number of neutrophils following a similar trend. The accumulation of infiltrating cells across the observation window was compared in Fig. 10F and G and showed that the significant increase in immune cell infiltrate between day 4 and day 8 was abolished with microneedle treatment. This demonstrates the dampening effect of the IL-10 and ATRA microneedle patch on the accumulation of pro-inflammatory cell populations in the IMQ mouse model which led to the reduced clinical score reported in Fig. 5. This is also in line with DAPI mean fluorescence intensity in Fig. 9.

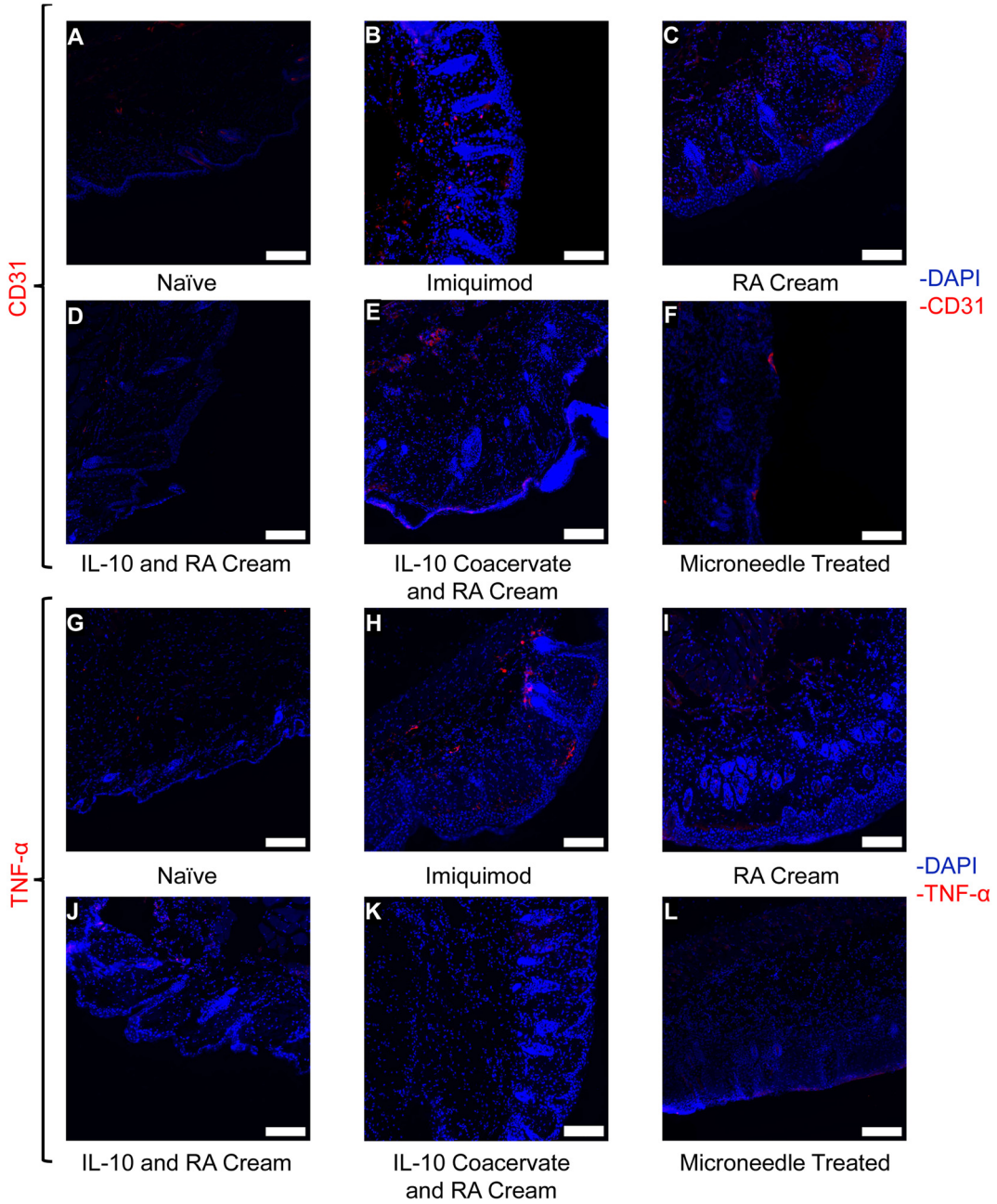


**Fig. 9** Immunofluorescence of mouse skin with CD31 and TNF-α on day 4. CD31, or PECAM-1, immunofluorescence is shown in A–F. TNF-α IHC is shown in G–L. All skin samples were stained with DAPI to label nuclei of cells. Scale bar: 100 μm.

## 4. Discussion

Psoriasis is a prevalent autoimmune disease that imposes significant health burdens to individuals and healthcare systems.[3,34] Current first-line psoriasis treatments include retinoids, corticosteroids, vitamin D analogues and light therapy.[17] While recent advancements have introduced various biological treatment options, these require systemic immunosuppression, increasing risk of infection, cancer, and other diseases.[34–36] There is a critical need for treatments to avoid these deleterious side effects through improved targeting and providing alternatives for patients who fail to respond to current therapies.

Alternative delivery methods such as nanoparticles and liposomal carriers have been explored to increase delivery across the stratum corneum which limits many topical treatments.[37,38] No such treatments have translated clinically with recent FDA authorizations being biological options.[39,40] Other efforts have been made to explore combination therapies to circumvent negative side effects or to increase the effectiveness of treatment.[3,37] Microneedles offer a painless delivery method for a wide range of biological compounds including

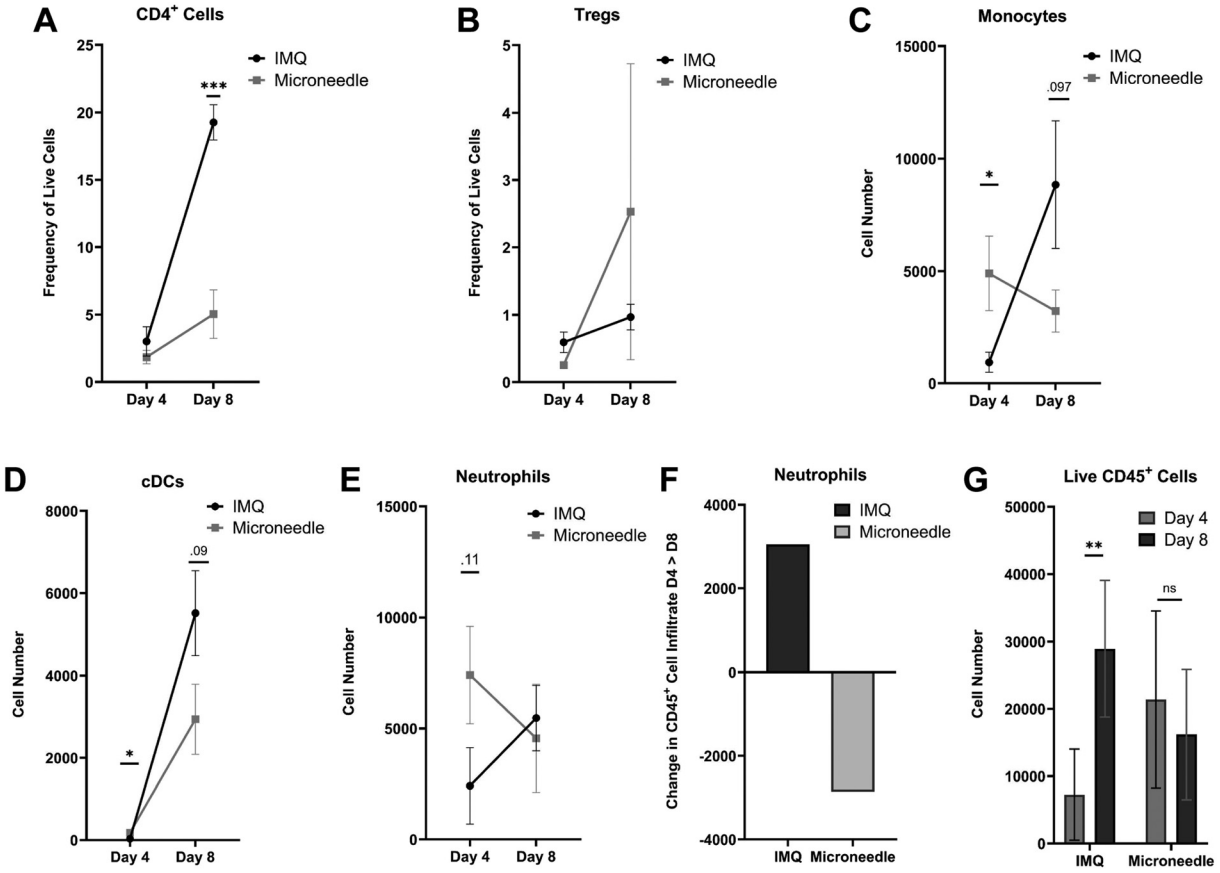


**Fig. 10** Flow cytometry analysis of T cells (A and B) and myeloid cells of interest (C–E) after imiquimod application with or without microneedle treatment ($n$ = 5). Changes in cell infiltrate are also shown (F and G). Despite an initially higher neutrophil count on day 4, by day 8 cell infiltrates were decreased within the microneedle treated mice. SEM shown.

vaccines, insulin, and antibodies.[41–44] The ability of microneedles to deliver potent biologics holds great promise for the treatment of autoimmune and infectious diseases.[45] Additionally, microneedles have been used to deliver retinoic acid for actinic keratosis, lentigo, atrophic scar, or photo-aged skin.[13,46,47] We sought to leverage this platform for a novel combination therapy of both a biologic and a small molecule. By incorporating coacervate into a microneedle, a first for the technology, we aimed to enhance the stability of encapsulated proteins and biologic compounds.

We developed a dual modality spatially localized delivery system to administer immunotherapeutics directly to psoriatic skin without systemic exposure. This platform utilizes biological and small molecules to simultaneously target multiple drivers of the disease. To address T cell activity, Treg stability, and keratinocyte hyperproliferation, we delivered Interleukin-10 (IL-10) and all-*trans* retinoic acid (ATRA) across the cutaneous barrier. These two molecules have known anti-inflammatory effects for the immune signaling pathways involved in psoriasis. The microneedle architecture facilitates this through a staged release: the rapid dissolution of a polyvinyl pyrrolidone (PVP) matrix deploys IL-10 encapsulated coacervates for sustained delivery, while ATRA is released from a secondary microneedle layer.

We first validated the incorporation of coacervate into a microneedle, a novel approach for the delivery of these droplets whilst protecting unstable proteins.[20–22] SEM and mechanical testing demonstrated that the microneedles maintained their desired structure and were capable of skin penetration.[48] The introduction of coacervate significantly decreases mechanical strength. Unfortunately, this weakness limits polymer selection and requires high-molecular-weight polyvinyl pyrrolidone (PVP) to meet mechanical requirements for skin penetration. Minimum skin penetration strength is achieved by increasing the amount of PVP used in microneedle fabrications from 2.5% to 5%. The large decrease in strength of 10% PVP with the introduction of coacervate suggests coacervate may interfere with chain entanglement of PVP. This may also explain the large difference in strength between 10% and 5% PVP solutions. This design was used for subsequent *in vivo* testing.

Imiquimod (IMQ) is a TLR7/8 agonist, known for reliably inducing psoriasiform skin in mice.[26,27] Using the microneedle treatment on IMQ treated C57BL/6 mice, we ameliorated markers of PASI caused by IMQ. Across the treatment groups, the microneedle treatment did not show significant improvement across early timepoints. Skin thickness was measured on

days 4, and 8 using H&E stained samples from each of the groups. The decreased thickening in IL-10 treated models matches the results seen visually using PASI measurements. Moreover, we confirmed the decreased response to IMQ using immunostaining for TNF-α, a common pro-inflammatory cytokine associated with worse patient outcomes, and CD31, a marker for vascularization of skin tissues. Abnormal and excessive vascularization of the tissues is correlated with poor disease outcomes.[49] Indeed, other treatments of psoriasis have also displayed a decrease in CD31 in diseased tissue in response to methotrexate.[50] We therefore conclude that the decrease in both CD31 and TNF-α correlates with a partial control of skin pathology triggered by IMQ. We then expanded upon this work to investigate the individual effects on immune cell populations within inflamed skin.

To further investigate the effect of the treatment and accumulation of immune cells within the tissue, we analyzed the skin using flow cytometry. Flow cytometry revealed shifts in the cell infiltration into the cutaneous tissue, namely a decrease in the number of neutrophils and total number of $CD4^+$ T cells. Neutrophils are a known contributor to disease and a major source of IL-17 production within psoriasis. $CD4^+$ T cells also contribute to the production of IL-17, commonly taking on the Th17 phenotype in psoriasis. Limiting the infiltration of these immune cells into cutaneous tissues is likely one of the key factors in disease prevention over the course of IMQ application.

While the treatment significantly improved disease markers, it did not fully halt progression. The surge in neutrophil infiltration observed on day 4 may be triggered by the microneedle application on day 2. Microneedles are known to generate a sterile immune response, and it is possible that only the end of the response is seen on day 4 but is corrected by day 8 due to IL-10 and ATRA.[51,52] This also aligns with the higher TNF-α MFI measurements on day 4 compared to day 8. Early PASI scores of microneedle treatment do not show significant improvement over other groups. This is seen in MFI values of the samples as well but by day 8 the large changes to disease progression have become clearer.

Furthermore, early damage may also result in an increased proliferation of anti-inflammatory macrophages leading to an improved response similar to what is seen in narrow-band ultraviolet B therapy.[53–55] Additional exploration with scRNA-Seq would reveal the subtle changes in macrophage population if any exist. Investigation of various microneedle geometries should also be done to minimize adverse effects caused by larger needles. It was also found there was not a significant response increase in the percentage of Treg $CD4^+$, further work could explore increasing the dosage of ATRA. This could help generate stable Tregs for resolution of the disease.

Immunotherapies have great potential not only for psoriasis, but also for autoimmune diseases, cancers and allergies. There is a growing need for treatments for autoimmune disorders as prevalence continues to increase.[56] Personalized medicine holds promise to facilitate improvements of outcomes and quality of life, however, more targeted treatment strategies are needed. This microneedle therapy, while targeted to psoriasis, has many potential benefits that can be leveraged in future treatments. The potent combination of biologics and small molecules in a localized treatment limits toxic systemic effects often seen with immunotherapies. Future work done should focus on minimizing unwanted inflammation caused by microneedle insertion followed by greater control of the release of RA and IL-10 to ensure maximum bioactivity. Additionally, pharmacokinetics will give a deeper insight into treatment efficacy.

## 5. Conclusions

We have designed a multilayered microneedle to deliver biologics and small molecules simultaneously for the treatment of psoriasis. The outermost layer contains IL-10 encapsulated in a coacervate to control its release over time while preserving its secondary structure and bioactivity. The second layer is designed to degrade and dissolve allowing for simultaneous delivery of ATRA by microneedles. This strategy combines two treatment modalities into one with a therapeutic outcome matching the PASI score of IL-10-coacervate injection and topical treatment of ATRA cream, but with a superior skin architecture. Without the protection of coacervate, free IL-10 protein combined with ATRA cream shows little improvement. Flow cytometry on cell populations within the cutaneous tissue reveals a decrease in infiltrating immune cells upon microneedle treatment leading to decreased disease progression. The microneedle is expected to be painless, protect the bioactivity of IL-10 and lower key markers of psoriasis in the IMQ model. Therefore, this microneedle system is potentially highly useful for immunotherapies and warrants further exploration in psoriasis and other diseases.

## Conflicts of interest

The authors declare that they have no conflict of interest.

## Data availability

Data from the study are available upon reasonable request from the corresponding author.

Supplementary information (SI) is available. Includes additional statistical information and fluorescence data. See DOI: https://doi.org/10.1039/d5pm00233h.

## Acknowledgements

This work made use of the Cornell Center for Materials Research Shared Facilities which are supported through the NSF MRSEC program (DMR-1719875). This work was supported by a Cornell startup grant (YW).

## References

1 F. O. Nestle, D. H. Kaplan and J. Barker, Psoriasis, *N. Engl. J. Med.*, 2009, **361**(5), 496–509, DOI: 10.1056/NEJMra0804595.
2 E. Ogawa, Y. Sato, A. Minagawa and R. Okuyama, Pathogenesis of Psoriasis and Development of Treatment, *J. Dermatol.*, 2018, **45**(3), 264–272, DOI: 10.1111/1346-8138.14139.
3 A. Rendon and K. Schäkel, Psoriasis Pathogenesis and Treatment, *Int. J. Mol. Sci.*, 2019, **20**(6), 1475, DOI: 10.3390/ijms20061475.
4 T. Liu, S. Li, S. Ying, S. Tang, Y. Ding, Y. Li, J. Qiao and H. Fang, The IL-23/IL-17 Pathway in Inflammatory Skin Diseases: From Bench to Bedside, *Front. Immunol.*, 2020, **11**, 594735.
5 L. I. Ortiz-Lopez, V. Choudhary and W. B. Bollag, Updated Perspectives on Keratinocytes and Psoriasis: Keratinocytes Are More Than Innocent Bystanders, *Psoriasis: Targets Ther.*, 2022, **12**, 73–87, DOI: 10.2147/PTT.S327310.
6 M. H. Braff, M. Zaiou, J. Fierer, V. Nizet and R. L. Gallo, Keratinocyte Production of Cathelicidin Provides Direct Activity against Bacterial Skin Pathogens, *Infect. Immun.*, 2005, **73**(10), 6771–6781, DOI: 10.1128/IAI.73.10.6771-6781.2005.
7 S. S. Iyer and G. Cheng, Role of Interleukin 10 Transcriptional Regulation in Inflammation and Autoimmune Disease, *Crit. Rev. Immunol.*, 2012, **32**(1), 23–63.
8 V. Carlini, D. M. Noonan, E. Abdalalem, D. Goletti, C. Sansone, L. Calabrone and A. Albini, The Multifaceted Nature of IL-10: Regulation, Role in Immunological Homeostasis and Its Relevance to Cancer, COVID-19 and Post-COVID Conditions, *Front. Immunol.*, 2023, **14**, 1161067.
9 D. S. Shouval, J. Ouahed, A. Biswas, J. A. Goettel, B. H. Horwitz, C. Klein, A. M. Muise and S. B. Snapper, Interleukin 10 Receptor Signaling: Master Regulator of Intestinal Mucosal Homeostasis in Mice and Humans, *Adv. Immunol*, 2014, **122**, 177–210, DOI: 10.1016/B978-0-12-800267-4.00005-5.
10 K. Asadullah, W.-D. Döcke, M. Ebeling, M. Friedrich, G. Belbe, H. Audring, H.-D. Volk and W. Sterry, Interleukin 10 Treatment of Psoriasis: Clinical Results of a Phase 2 Trial, *Arch. Dermatol.*, 1999, **135**(2), 187–192, DOI: 10.1001/archderm.135.2.187.
11 A. B. Kimball, T. Kawamura, K. Tejura, C. Boss, A. R. Hancox, J. C. Vogel, S. M. Steinberg, M. L. Turner and A. Blauvelt, Clinical and Immunologic Assessment of Patients With Psoriasis in a Randomized, Double-Blind, Placebo-Controlled Trial Using Recombinant Human Interleukin 10, *Arch. Dermatol.*, 2002, **138**(10), 1341–1346, DOI: 10.1001/archderm.138.10.1341.
12 W. Hong and L. Itri, *Retinoids and Human Cancer*, Raven Press, New York, 2nd edn, 1994.
13 Y. Hiraishi, S. Hirobe, H. Iioka, Y.-S. Quan, F. Kamiyama, H. Asada, N. Okada and S. Nakagawa, Development of a Novel Therapeutic Approach Using a Retinoic Acid-Loaded Microneedle Patch for Seborrheic Keratosis Treatment and Safety Study in Humans, *J. Controlled Release*, 2013, **171**(2), 93–103, DOI: 10.1016/j.jconrel.2013.06.008.
14 Y. Nozaki, T. Yamagata, M. Sugiyama, S. Ikoma, K. Kinoshita and M. Funauchi, Anti-Inflammatory Effect of All-Trans-Retinoic Acid in Inflammatory Arthritis, *Clin. Immunol.*, 2006, **119**(3), 272–279, DOI: 10.1016/j.clim.2005.11.012.
15 L. d. M. Oliveira, F. M. E. Teixeira and M. N. Sato, Impact of Retinoic Acid on Immune Cells and Inflammatory Diseases, *Mediators Inflammation*, 2018, **2018**, 3067126, DOI: 10.1155/2018/3067126.
16 D.-D. Lee, O. Stojadinovic, A. Krzyzanowska, C. Vouthounis, M. Blumenberg and M. Tomic-Canic, Retinoid-Responsive Transcriptional Changes in Epidermal Keratinocytes, *J. Cell. Physiol.*, 2009, **220**(2), 427–439, DOI: 10.1002/jcp.21784.
17 C. A. Elmets, N. J. Korman, E. F. Prater, E. B. Wong, R. N. Rupani, D. Kivelevitch, A. W. Armstrong, C. Connor, K. M. Cordoro, D. M. R. Davis, B. E. Elewski, J. M. Gelfand, K. B. Gordon, A. B. Gottlieb, D. H. Kaplan, A. Kavanaugh, M. Kiselica, D. Kroshinsky, M. Lebwohl, C. L. Leonardi, J. Lichten, H. W. Lim, N. N. Mehta, A. S. Paller, S. L. Parra, A. L. Pathy, M. Siegel, B. Stoff, B. Strober, J. J. Wu, V. Hariharan and A. Menter, Joint AAD–NPF Guidelines of Care for the Management and Treatment of Psoriasis with Topical Therapy and Alternative Medicine Modalities for Psoriasis Severity Measures, *J. Am. Acad. Dermatol.*, 2021, **84**(2), 432–470, DOI: 10.1016/j.jaad.2020.07.087.
18 F. Kerdel and M. Zaiac, An Evolution in Switching Therapy for Psoriasis Patients Who Fail to Meet Treatment Goals, *Dermatol. Ther.*, 2015, **28**(6), 390–403, DOI: 10.1111/dth.12267.
19 M. Augustin, A. B. Gottlieb, M. Lebwohl, A. Pinter, R. B. Warren, L. Puig, R. Warham, J. Lambert, S. Wiegratz, B. Szilagyi and A. Blauvelt, Complete Skin Clearance Is Associated with the Greatest Benefits to Health-Related Quality of Life and Perceived Symptoms for Patients with Psoriasis, *Dermatol. Ther.*, 2024, **14**(10), 2841–2857, DOI: 10.1007/s13555-024-01261-6.
20 M. P. Hwang, R. J. Fecek, T. Qin, W. J. Storkus and Y. Wang, Single Injection of IL-12 Coacervate as an Effective Therapy Against B16-F10 Melanoma in Mice, *J. Controlled Release*, 2020, **318**, 270–278, DOI: 10.1016/j.jconrel.2019.12.035.
21 W. C. W. Chen, B. G. Lee, D. W. Park, K. Kim, H. Chu, K. Kim, J. Huard and Y. Wang, Controlled Dual Delivery of Fibroblast Growth Factor-2 and Interleukin-10 by Heparin-Based Coacervate Synergistically Enhances Ischemic Heart Repair, *Biomaterials*, 2015, **72**, 138–151, DOI: 10.1016/j.biomaterials.2015.08.050.
22 X. Gao, M. P. Hwang, N. Wright, A. Lu, J. J. Ruzbarsky, M. Huard, H. Cheng, M. Mullen, S. Ravuri, B. Wang, Y. Wang and J. Huard, The Use of Heparin/Polycation Coacervate Sustain Release System to Compare the Bone

Regenerative Potentials of 5 BMPs Using a Critical Sized Calvarial Bone Defect Model, *Biomaterials*, 2022, **288**, 121708, DOI: 10.1016/j.biomaterials.2022.121708.

23 N. R. Johnson and Y. Wang, Coacervate Delivery of HB-EGF Accelerates Healing of Type 2 Diabetic Wounds, *Wound Repair Regen.*, 2015, **23**(4), 591–600, DOI: 10.1111/wrr.12319.

24 N. Wright, T. Wu and Y. Wang, Multilayered Microneedles for Triphasic Controlled Delivery of Small Molecules and Proteins, *Macromol. Biosci.*2300431, DOI: 10.1002/mabi.202300431.

25 X. Ding, P. G. Miller, M. P. Hwang, J. Fu and Y. Wang, Scale-up Synthesis of a Polymer Designed for Protein Therapy, *Eur. Polym. J.*, 2019, **117**, 353–362, DOI: 10.1016/j.eurpolymj.2019.05.032.

26 L. van der Fits, S. Mourits, J. S. A. Voerman, M. Kant, L. Boon, J. D. Laman, F. Cornelissen, A.-M. Mus, E. Florencia, E. P. Prens and E. Lubberts, Imiquimod-Induced Psoriasis-Like Skin Inflammation in Mice Is Mediated via the IL-23/IL-17 Axis1, *J. Immunol.*, 2009, **182**(9), 5836–5845, DOI: 10.4049/jimmunol.0802999.

27 M. Jabeen, A.-S. Boisgard, A. Danoy, N. El Kholti, J.-P. Salvi, R. Boulieu, B. Fromy, B. Verrier and M. Lamrayah, Advanced Characterization of Imiquimod-Induced Psoriasis-Like Mouse Model, *Pharmaceutics*, 2020, **12**(9), 789, DOI: 10.3390/pharmaceutics12090789.

28 J. S. Kochhar, T. C. Quek, W. J. Soon, J. Choi, S. Zou and L. Kang, Effect of Microneedle Geometry and Supporting Substrate on Microneedle Array Penetration into Skin, *J. Pharm. Sci.*, 2013, **102**(11), 4100–4108, DOI: 10.1002/jps.23724.

29 S. D. Gittard, B. Chen, H. Xu, A. Ovsianikov, B. N. Chichkov, N. A. Monteiro-Riviere and R. J. Narayan, The Effects of Geometry on Skin Penetration and Failure of Polymer Microneedles, *J. Adhes. Sci. Technol.*, 2013, **27**(3), 227–243, DOI: 10.1080/01694243.2012.705101.

30 A. Micsonai, F. Wien, L. Kernya, Y. H. Lee, Y. Goto, M. Réfrégiers and J. Kardos, Accurate secondary structure prediction and fold recognition for circular dichroism spectroscopy, *Proc. Natl. Acad. Sci. U. S. A.*, 2015, **112**, E3095–E3103, https://www.pnas.org/doi/10.1073/pnas.1500851112 (accessed 02-02-2024 ).

31 M. Rodgers, D. Epstein, L. Bojke, H. Yang, D. Craig, T. Fonseca, L. Myers, I. Bruce, R. Chalmers, S. Bujkiewicz, M. Lai, N. Cooper, K. Abrams, D. Spiegelhalter, A. Sutton, M. Sculpher and N. Woolacott, Estimation of Psoriasis Area and Severity Index Score for Treatment Responders in the Decision Model, in *Etanercept, Infliximab and Adalimumab for the Treatment of Psoriatic Arthritis: A Systematic Review and Economic Evaluation*, NIHR Journals Library, 2011.

32 S. von Csiky-Sessoms, J. C. D. Rosa, J. Han, D. Dubin and M. Lebwohl, The Reliability of Disease Severity Assessment in Psoriasis Patients of Color: Results of an Educational Intervention, *J. Am. Acad. Dermatol.*, 2023, **88**(4), 895–897, DOI: 10.1016/j.jaad.2022.10.025.

33 H. Prizant, N. Patil, S. Negatu, N. Bala, A. McGurk, S. A. Leddon, A. Hughson, T. D. McRae, Y.-R. Gao, A. M. Livingstone, J. R. Groom, A. D. Luster and D. J. Fowell, CXCL10+ Peripheral Activation Niches Couple Preferred Sites of Th1 Entry with Optimal APC Encounter, *Cell Rep.*, 2021, **36**(6), 109523, DOI: 10.1016/j.celrep.2021.109523.

34 C. E. M. Griffiths, A. W. Armstrong, J. E. Gudjonsson and J. N. W. N. Barker, Psoriasis, *Lancet*, 2021, **397**(10281), 1301–1315, DOI: 10.1016/S0140-6736(20)32549-6.

35 U. U. Mohd Nordin, N. Ahmad, N. Salim and N. S. Mohd Yusof, Lipid-Based Nanoparticles for Psoriasis Treatment: A Review on Conventional Treatments, Recent Works, and Future Prospects, *RSC Adv.*, 2021, **11**(46), 29080–29101, DOI: 10.1039/d1ra06087b.

36 L. Hoisnard, B. Lebrun-Vignes, S. Maury, M. Mahevas, K. El Karoui, L. Roy, A. Zarour, M. Michel, J. L. Cohen, A. Amiot, P. Claudepierre, P. Wolkenstein, P. Grimbert and E. Sbidian, Adverse Events Associated with JAK Inhibitors in 126,815 Reports from the WHO Pharmacovigilance Database, *Sci. Rep.*, 2022, **12**(1), 7140, DOI: 10.1038/s41598-022-10777-w.

37 W. Wang, G. Shu, K. Lu, X. Xu, M. Sun, J. Qi, Q. Huang, W. Tan and Y. Du, Flexible Liposomal Gel Dual-Loaded with All-Trans Retinoic Acid and Betamethasone for Enhanced Therapeutic Efficiency of Psoriasis, *J. Nanobiotechnol.*, 2020, **18**(1), 80, DOI: 10.1186/s12951-020-00635-0.

38 Y. O. Agrawal, U. B. Mahajan, H. S. Mahajan and S. Ojha, Methotrexate-Loaded Nanostructured Lipid Carrier Gel Alleviates Imiquimod-Induced Psoriasis by Moderating Inflammation: Formulation, Optimization, Characterization, In-Vitro and In-Vivo Studies, *Int. J. Nanomed.*, 2020, **15**, 4763–4778, DOI: 10.2147/IJN.S247007.

39 U.S. FDA approves TREMFYA® (guselkumab) for the treatment of pediatric plaque psoriasis and active psoriatic arthritis, marking a first and only approval for an IL-23 inhibitor. JNJ.com. https://www.jnj.com/media-center/press-releases/u-s-fda-approves-tremfya-guselkumab-for-the-treatment-of-pediatric-plaque-psoriasis-and-active-psoriatic-arthritis-marking-a-first-and-only-approval-for-an-il-23-inhibitor (accessed 16-02-2026).

40 FDA Approves Skyrizi for Plaque Psoriasis. https://www.psoriasis.org/advance/fda-approves-skyrizi-for-plaque-psoriasis/ (accessed 16-02-2026).

41 Y. Choi, G. S. Lee, S. Li, J. W. Lee, T. Mixson-Hayden, J. Woo, D. Xia, M. R. Prausnitz, S. Kamili, M. A. Purdy and R. A. Tohme, Hepatitis B Vaccine Delivered by Microneedle Patch: Immunogenicity in Mice and Rhesus Macaques, *Vaccine*, 2023, **41**(24), 3663–3672, DOI: 10.1016/j.vaccine.2023.05.005.

42 Q. Chen, Z. Xiao, C. Wang, G. Chen, Y. Zhang, X. Zhang, X. Han, J. Wang, X. Ye, M. R. Prausnitz, S. Li and Z. Gu, Microneedle Patches Loaded with Nanovesicles for Glucose Transporter-Mediated Insulin Delivery, *ACS Nano*, 2022, **16**(11), 18223–18231, DOI: 10.1021/acsnano.2c05687.

43 K. T. M. Tran, T. T. Le, V. Agrahari, M. M. Peet, L. A. Ouattara, S. M. Anderson, T. H. Le-Kim, O. N. Singh,

G. F. Doncel and T. D. Nguyen, Single-Administration Long-Acting Microarray Patch with Ultrahigh Loading Capacity and Multiple Releases of Thermally Stable Antibodies, *Mol. Pharm.*, 2023, **20**(5), 2352–2361, DOI: 10.1021/acs.molpharmaceut.2c00919.

44 A. Romanyuk, R. Wang, A. Marin, B. M. Janus, E. I. Felner, D. Xia, Y. Goez-Gazi, K. J. Alfson, A. S. Yunus, E. A. Toth, G. Ofek, R. Carrion, M. R. Prausnitz, T. R. Fuerst and A. K. Andrianov, Skin Vaccination with Ebola Virus Glycoprotein Using a Polyphosphazene-Based Microneedle Patch Protects Mice against Lethal Challenge, *J. Funct. Biomater.*, 2022, **14**(1), 16, DOI: 10.3390/jfb14010016.

45 H. Amani, M.-A. Shahbazi, C. D'Amico, F. Fontana, S. Abbaszadeh and H. A. Santos, Microneedles for Painless Transdermal Immunotherapeutic Applications, *J. Controlled Release*, 2021, **330**, 185–217, DOI: 10.1016/j.jconrel.2020.12.019.

46 S. Hirobe, R. Otsuka, H. Iioka, Y.-S. Quan, F. Kamiyama, H. Asada, N. Okada and S. Nakagawa, Clinical Study of a Retinoic Acid-Loaded Microneedle Patch for Seborrheic Keratosis or Senile Lentigo, *Life Sci.*, 2017, **168**, 24–27, DOI: 10.1016/j.lfs.2015.12.051.

47 B. Limcharoen, P. Toprangkobsin, M. Kröger, M. E. Darvin, T. Sansureerungsikul, T. Rutwaree, S. Wanichwecharungruang, W. Banlunara, J. Lademann and A. Patzelt, Microneedle-Facilitated Intradermal Proretinal Nanoparticle Delivery, *Nanomaterials*, 2020, **10**(2), 368, DOI: 10.3390/nano10020368.

48 X. Jiang and P. B. Lillehoj, Microneedle-Based Skin Patch for Blood-Free Rapid Diagnostic Testing, *Microsyst. Nanoeng.*, 2020, **6**(1), 1–11, DOI: 10.1038/s41378-020-00206-1.

49 N. Chawla, S. P. Kataria, K. Aggarwal, P. Chauhan and D. Kumar, Significance of Vascular Endothelial Growth Factor and CD31 and Morphometric Analysis of Microvessel Density by CD31 Receptor Expression as an Adjuvant Tool in Diagnosis of Psoriatic Lesions of Skin, *Indian J. Pathol. Microbiol.*, 2017, **60**(2), 189–195, DOI: 10.4103/IJPM.IJPM_862_15.

50 E. Zemheri, A. S. Karadağ, I. Zindancı, P. E. Zerk and M. K. Ozturk, Evaluation of Microvessel Density with CD31 and CD105 in Patients with Psoriasis under Methotrexate and Acitretin Therapy, *Postepy Dermatol. Alergol.*, 2020, **37**(3), 422–427, DOI: 10.5114/ada.2019.87279.

51 C. Edwards, S. A. Shah, T. Gebhardt and C. M. Jewell, Exploiting Unique Features of Microneedles to Modulate Immunity, *Adv. Mater.*, 2023, **35**(52), e2302410, DOI: 10.1002/adma.202302410.

52 Y. Han, X. Qin, W. Lin, C. Wang, X. Yin, J. Wu, Y. Chen, X. Chen and T. Chen, Microneedle-Based Approaches for Skin Disease Treatment, *Nano-Micro Lett.*, 2025, **17**, 132, DOI: 10.1007/s40820-025-01662-y.

53 P. Zhang and M. X. Wu, A Clinical Review of Phototherapy for Psoriasis, *Lasers Med. Sci.*, 2018, **33**(1), 173–180, DOI: 10.1007/s10103-017-2360-1.

54 L. Zhang, Type1 Interferons Potential Initiating Factors Linking Skin Wounds With Psoriasis Pathogenesis, *Front. Immunol.*, 2019, **10**, 1440.

55 L. Kemény, E. Varga and Z. Novak, Advances in Phototherapy for Psoriasis and Atopic Dermatitis, *Expert Rev. Clin. Immunol.*, 2019, **15**(11), 1205–1214, DOI: 10.1080/1744666X.2020.1672537.

56 N. Conrad, S. Misra, J. Y. Verbakel, G. Verbeke, G. Molenberghs, P. N. Taylor, J. Mason, N. Sattar, J. J. V. McMurray, I. B. McInnes, K. Khunti and G. Cambridge, Incidence, prevalence, and co-occurrence of autoimmune disorders over time and by age, sex, and socioeconomic status: a population-based cohort study of 22 million individuals in the UK, *Lancet*, 2023, **401**, 1878–1890, https://www.thelancet.com/journals/lancet/article/PIIS0140-6736(23)00457-9/fulltext (accessed 01-01-2024).